Unusual local disorder in NdOs_{4}Sb_{12} and PrOs_{4}Sb_{12} skutterudites

T. Keiber, F. Bridges, R. E. Baumbach, and M. B. Maple

Phys. Rev. B **86**, 174106 — Published 9 November 2012

DOI: 10.1103/PhysRevB.86.174106

Unusual local disorder in $NdOs_4Sb_{12}$ and $PrOs_4Sb_{12}$ Skutterudites

T. Keiber,[1] F. Bridges,[1] R. E. Baumbach,[2] and M. B. Maple[3]

[1] *Physics Department, University of California, Santa Cruz, California 95064, USA*
[2] *Los Alamos National Laboratory, New Mexico, USA*
[3] *Physics Department, University of California, San Diego, California, USA*

(Dated: October 15, 2012)

We present a temperature-dependent, extended x-ray absorption fine structure (EXAFS) analysis of the filled skutterudite compounds $NdOs_4Sb_{12}$, $PrOs_4Sb_{12}$ and $EuOs_4Sb_{12}$. Although the interpretation of recent ultrasonic measurements suggested off-center displacements for Nd and Pr in $NdOs_4Sb_{12}$ and $PrOs_4Sb_{12}$, the EXAFS analysis shows that the Nd-Sb, Pr-Sb, and Sb-Sb peaks are well ordered. Surprisingly however, the second neighbor Nd-Os and Pr-Os peaks are highly disordered, even at low temperatures, and the Os-Os peak also has some disorder in the Nd and Pr systems. In contrast to the anomalous results for the Pr and Nd samples, neither the Eu-Sb, Eu-Os, nor the Os-Os peak is disordered at low temperature for $EuOs_4Sb_{12}$. For all three systems within estimated errors, the rare earth atom is on-center inside the Sb cage. We propose that for the Nd and Pr compounds, the Os cage distorts, with some of the Os atoms moving either towards or away from the Nd or Pr atoms, such that the Nd-Sb, Pr-Sb and Sb-Sb pair distances have very little disorder. Some possible distortion models are suggested and the possible ramifications for thermoelectric and transport properties are discussed.

I. INTRODUCTION

The family of filled skutterudite compounds with the chemical formula LnT_4X_{12} (Ln = lanthanide; T = Fe, Ru, or Os; and X = P, As, or Sb) displays an unusually wide variety of interesting phenomena including low thermal conductivity and good thermoelectric properties at high temperatures, 600-900 K,[1] conventional and unconventional superconductivity, magnetic and multipolar order, metal-insulator transitions, Kondo phenomena, heavy fermion (HF), and non-Fermi-liquid behavior.[2–5] These compounds crystallize in the cubic $Im\bar{3}$ space group, and are characterized by a large unit cell which includes icosahedral pnictogen (X) cages that surround the Ln ions. The crystal structure is shown in Fig. 1. It has been proposed that some of the exotic phenomena that are seen in these materials originate from this unusual atomic configuration, which allows the Ln ions to undergo large amplitude ("rattling") vibrations,[1] leading to strong phonon scattering and local charge degrees of freedom.[6,7] Correlated electron behavior is also generated by hybridization between the localized 4f electronic states of the Ln ions, and the conduction electron states. Crystalline electric field (CEF) splittings of the Hund's rule multiplets of the Ln ions also play an important role in the physical properties of these materials.[8–10]

A variety of experimental techniques have been used to investigate these materials, including extended X-ray absorption fine structure (EXAFS),[11–14] ultrasonic measurements,[15–17] specific heat,[18] Raman scattering,[19] inelastic neutron and X-ray scattering[20–22], nuclear inelastic scattering[23], and single crystal X-ray diffraction.[24] Many of these measurements reveal the presence of a low lying optical phonon, supporting the point of view that the Ln ions undergo a low energy rattling behavior about the crystallographic Ln site shown in Fig. 1.

However, two of the Sb-based filled skutterudites

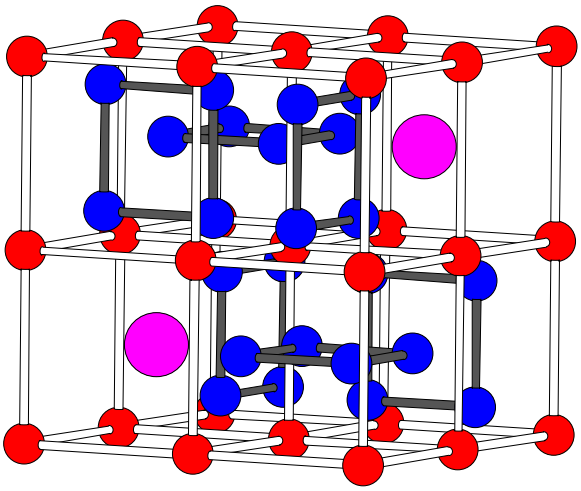

FIG. 1. The skutterudite unit cell. Large atoms (pink) - Ln; internal square rings (blue) - X atoms, here Sb; cubic cage structure (red) - T atoms.

$NdOs_4Sb_{12}$ and $PrOs_4Sb_{12}$, exhibit several unusual properties that may be related to distortions of the local structure: first, ultrasonic measurements have revealed a low temperature softening of the phonon dispersion, which has been interpreted in terms of large off-center displacements of the Nd and Pr ions.[15,16,25] The proposed off-center displacement for Nd is surprisingly large - 0.4 Å - twice as large as that suggested for Pr. In addition, unexpected HF behavior at low temperature is also observed for these materials, where γ is 520 mJ/mol-K^2 and $\sim$ 310 – 750 mJ/mol-K^2, respectively, for the Nd and Pr compounds, pointing towards the possibility of a common mechanism for the mass enhancement in this family of Sb-based crystals.[26,27] In contrast, a recent Sb-NMR study of $PrOs_4Sb_{12}$ suggests that in this case, the

mass enhancement[28] is due to scattering of the conduction electrons via multipole fluctuations that are related to the unusually small singlet-triplet crystal electric field (CEF) excitation.[29]

A prerequisite for developing models to describe the phonon scattering, the CEF and correlated electron behavior, is a clear understanding of the local structure, including possible local distortions and the lattice dynamics. Ultrasonic studies[15,16,25] are an indirect measure of local structure and a local probe is needed to clarify the structure. The EXAFS technique is particularly well suited to this effort because it provides an element specific method for determining interatomic distances and local distortions. Measurements as a function of temperature provide information about the dynamics for various atomic pairs, parametrized by the correlated Debye and/or Einstein temperatures.

Here we use the EXAFS technique to investigate the local structure in $NdOs_4Sb_{12}$ and $PrOs_4Sb_{12}$, for several shells of neighbors about each type of atom in the structure, and contrast those results with comparable measurements for $EuOs_4Sb_{12}$ which has no significant local distortions. Because the proposed off-center displacement for Nd is much larger than for Pr, we often focus on the Nd sample. Our measurements reveal that relative to the Sb cage, both Nd and Pr are on-center, low-energy rattlers, with no evidence for any significant off-center displacement. Surprisingly however, we find that although the nearest neighbor peaks have typical amplitudes for low temperature data, the second neighbor peaks (Nd-Os and Pr-Os) are anomalously small at 4 K, and not observable at 300 K - the suppression of the second neighbor peak is largest for the Nd sample. In contrast, for $EuOs_44Sb_{12}$, both the Eu-Sb and Eu-Os peaks at low temperatures have reasonable amplitudes with little excess broadening; additional measurements at the Os L_{III}- and Sb K-edges also show no significant local distortions for the Eu sample.

These results indicate that for the Nd and Pr materials, there is some type of disorder that is related to the Os site which is absent for the Eu analogue. Additionally, measurements at the Os L_{III}-edge for the Nd and Pr samples also indicate an anomaly for the Os-Os pair. Based on these results, we suggest several scenarios to model the disorder. This disorder is likely the reason for the anomalous results in ultrasonic measurements and may help clarify the unusual heavy fermion behavior and unconventional superconductivity in $PrOs_4Sb_{12}$.

II. EXPERIMENTAL DETAILS AND EXAFS TECHNIQUE

Single crystal samples of $LnOs_4Sb_{12}$ (Ln = Nd, Pr, Eu) were grown using a molten-metal flux method.[30] The samples were etched in a 1:1 HNO_3-HCl mixture to remove excess Sb flux.

EXAFS samples were prepared by grinding single crystals using a mortar and pestle. Next the powder was passed through a 400 mesh sieve and brushed onto scotch tape, which preferentially holds the smaller grains ($\leq 5\mu$m) in a thin layer. Two layers of tape were pressed together (double layer) to encapsulate the powder. For the low energy Ln L_{III}-edges, 2-3 double layers were used, while for the Os L_{III}-edge, 3-4 layers were used. Finally, for the high energy Sb K-edge ($\sim$ 30 keV) 8-12 layers were used.

TABLE I. Si double monochromator details: Beamline 10-2 has been upgraded to use liquid nitrogen (LN) cooled monochromator crystals, while beamline 4 (4-1, 4-2, 4-3) was moved to a different location and also upgraded to LN cooled crystals. Data were collected both before and after the upgrades. In the beamline column, "a" refers to the new configuration, while "b" refers to the old, water-cooled configuration.

Element	Slit Height (mm)	Crystals	Resolution (eV)	Beamline
$NdOs_4Sb_{12}$				
Nd	0.5	111	1.2	10-2a
Os	0.5	111	2.2	10-2a
Sb	0.2	220	3.2	10-2a
$PrOs_4Sb_{12}$				
Pr	1.5	220	0.9	4-3b
Os	0.7	220	1.4	4-3b
Sb	0.3	400	3	4-2b
$EuOs_4Sb_{12}$				
Eu	1.5	220	1.2	4-3b
Os	0.7	111	2.6	10-2b
Sb	0.3	220	4.7	4-3b

All the transmission EXAFS data were collected at the Stanford Synchrotron Radiation Laboratory (SSRL), over a wide temperature range (4-300 K) using Si monochromator crystals. Details of the beamline configuration used for each element are given in Table I. Most of the monochromators were detuned 50% to minimize harmonics. The exception is for the Sb K-edge for $NdOs_4Sb_{12}$; in this case, the monochromator was only detuned to 70%.

The EXAFS function for kχ(k) is a sum over neighboring shells and is given by[31]

$$k\chi(k) = \sum_{\mathrm{i}} k\chi_{\mathrm{i}}(k) = Im \sum_{\mathrm{i}} A_{\mathrm{i}} \int_0^\infty F_{\mathrm{i}}(k,r) \frac{g_{\mathrm{i}}(r_{0\mathrm{i}},r) e^{i(2kr+2\delta_{\mathrm{c}}(k)+\delta_{\mathrm{i}}(k))}}{r^2} dr \quad (1)$$

where r is the integration variable, $g_i(r_{0\mathrm{i}},r)$ is the i^{th} shell, pair distribution function (PDF), typically a Gaussian, for atoms at an average distance $r_{0\mathrm{i}}$ from the center atom, $F_{\mathrm{i}}(k,r)$ is the back scattering amplitude, and $\delta_{\mathrm{c}}(k)$ and $\delta_{\mathrm{i}}(k)$ are the phase shifts from the central and backscattering atom potentials respectively. The amplitude, A_{i}, is the product of the coordination number, N_{i}, from diffraction results and S_{o}^2, the amplitude reduction

factor, which is included to correct for multi-electron effects since multi-electron processes contribute to the edge step-height but not to the EXAFS amplitude. Experimentally, S_o^2 also corrects for several other small effects. Finally, an additional fitting parameter, $\Delta E_o/$, describes the difference in edge energy between the value defined for the data (energy at the half height position on the edge) and the theoretical functions (for which $k = 0$ at E_o). It is determined at low temperatures.

III. EXAFS DATA REDUCTION AND ANALYSIS

The EXAFS data were reduced using the RSXAP package.[32] First, a pre-edge background was subtracted from the data; the empirical Victoreen equations[33] were used such that for the subtracted data, the slope above the edge had the expected value. Next an experimental E_o was defined as the energy at the half-height point on each edge. The post-edge background μ_0 was obtained using a spline fit to the data above the edge and the EXAFS oscillations ($\chi(E)$) extracted using the equation $\mu(E) = \mu_0(1+\chi(E))$ where $\mu(E)$ is the absorption above the edge of interest. Next $\chi(E)$ was converted to k-space via the relation $k = \sqrt{\frac{2m(E-E_o)}{\hbar^2}}$, and the k-space data were Fourier transformed to yield r-space data. Examples of the k-space data for the Nd and Os L_{III}-edges and the Sb K-edge for $NdOs_4Sb_{12}$ are shown in Fig. 2.

To extract parameters such as bond lengths (r_i) and broadening (σ_i) of the pair distribution functions, fits of the EXAFS data were carried out in r-space, to a sum of theoretical functions, corresponding to different shells of neighboring atoms in the EXAFS equation. The theoretical functions for each atom pair, including some multiple-scattering (MS) paths, were calculated using FEFF8.[34] In this analysis we fit to both the real (Re) and imaginary (Im) parts of the Fourier Transform in r-space with some constraints included, as discussed below for specific samples and edges.

A. Rare earth L_{III}-edge data

The EXAFS r-space data at the L_{III}-edge for the rare earth elements, Nd, Pr, and Eu, are shown in Fig. 3 as a function of temperature; the temperature dependence is very strong for each sample, with the amplitude of all peaks decreasing rapidly as temperature increases. The Nd sample which has the largest proposed off-center rattler displacement is plotted at the top while the Eu sample which shows no significant disorder is at the bottom. For each rare earth atom, the first shell of neighbors is formed of twelve Sb atoms at ~ 3.5 Å from the Ln atom and the second shell of eight Os atoms at 4.0 Å- see Fig. 1. In EXAFS r-space plots, the positions of the peaks are shifted to shorter r by a well know phase factor for each atom pair, determined by the phase shifts $\delta_c(k)$ and $\delta_i(k)$.[35] The expected positions of the EXAFS r-space peaks are indicated by short vertical lines for each compound; these were determined using FEFF8[34] and the space group from diffraction.[2,27]

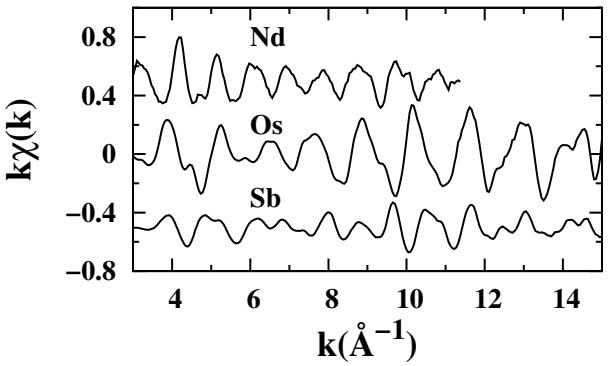

FIG. 2. Examples of k-space data at 4 K for the Nd and Os L_{III}-edges and at 8 K for the Sb K-edge in $NdOs_4Sb_{12}$, showing the high quality of the data. The corresponding data for $PrOs_4Sb_{12}$ and $EuOs_4Sb_{12}$ are similar. Note the k-range for the rare earth atoms is limited by the L_{II} edge.

Note the different FT ranges for each edge; the high end of the k-range is limited by the presence of the L_{II} edge - see Fig. 3 for details. The different FT ranges lead to different amplitudes in r-space; however if the same FT range (not shown) is used for comparison of the three samples at 4 K, the difference in amplitude of the first peak is ± 15%, and if modified using the measured values of S_o^2, the effective amplitudes only vary by ± 5%. Consquently the variation in σ at 4 K for the Nd-Sb, Pr-Sb and Eu-Sb pairs will be small.

The first double-peak structure for $NdOs_4Sb_{12}$ from 2.3-3.8 Å has a large amplitude at 4 K with a sharp dip near 3 Å; it is remarkably similar in shape to the Nd-Sb pair theoretical function calculated using FEFF8[34] which has maxima at 2.75 and 3.43 Å. Similar results are seen for the Pr and Eu L_{III} data. The similar shape and comparable amplitude when using the same FFT range indicates there is little distortion of the Nd-Sb and Pr-Sb peaks; the data are not consistent with Nd or Pr being significantly off-center. A further indication that there is little disorder of the first peak for any of the L_{III} data, is that the sharp dip near 3Å is observed for all three samples. If the pair distribution function were strongly broadened, this dip would almost disappear.

In contrast the second neighbor peaks for the Nd-Os and Pr-Os pairs, which should occur between roughly 3.5 and 4.3 Å, appear to be very weak at ~ 4 K, when compared to the Eu-Os peak. Since at low temperatures the thermal vibrations are reduced to zero-point-motion, a greatly reduced amplitude indicates significant static (or quasi-static) disorder, resulting in a large value for σ.

To investigate this in more detail, 2-peak fits of the 4 K data (a sum of Ln-Sb and Ln-Os functions) were

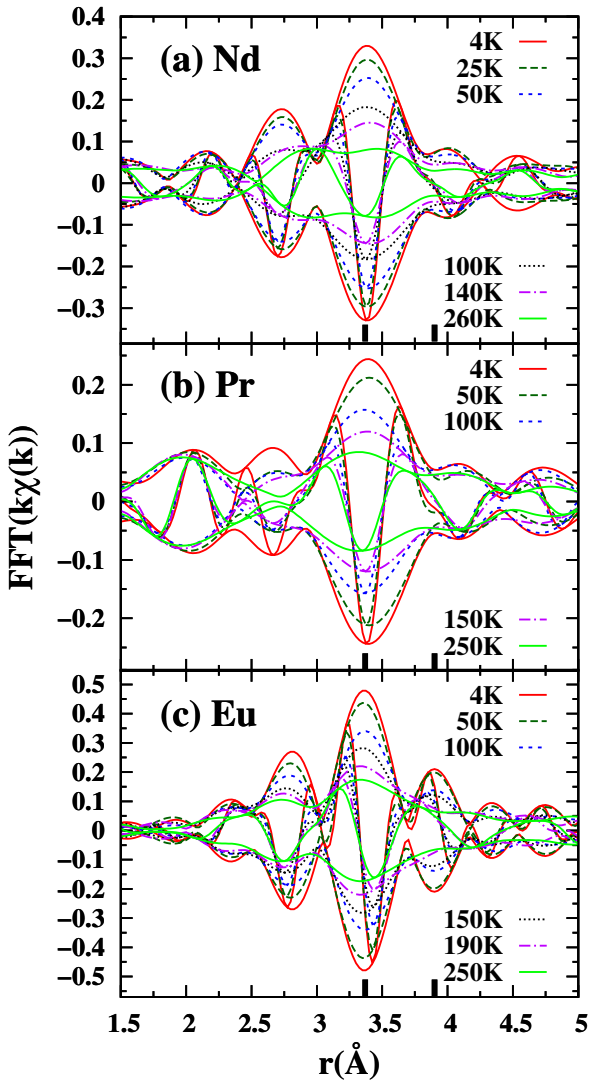

FIG. 3. Plots of the r-space data for the Nd, Pr, and Eu L_{III}-edges as a function of temperature, showing a strong temperature dependence. The expected positions of the first and second neighbors are indicated by short vertical black lines. Here, and in all r-space plots, the rapidly oscillating function is the real (Re) part of the FT while the envelope is given by $\sqrt{Re^2 + Im^2}$ where Im is the imaginary part of the FT. The FT ranges are: 3.5-10.2 Å^{-1} for Nd, 3.5-9.2 Å^{-1} for Pr and 3.5-11.2 Å^{-1} for Eu.

carried out from 2.5-4.3 Å for the Nd, Pr and Eu L_{III}-edges. For these fits at 4 K, we kept the amplitude ratio of the first Nd-Sb and Nd-Os pairs fixed at the ratio of the coordination numbers - 12:8, but varied the Nd-Sb amplitude to obtain S_o^2. We allowed five other parameters to vary: two δr's, two σ's and E_o (the energy at which k = 0 for the theoretical functions). The values of S_o^2 are 0.79, 0.75 and 0.96 for Nd, Pr, and Eu respectively. These fits are shown in Fig. 4, including the individual peaks.

For the Eu L_{III} edge, the Eu-Os peak has a moderate amplitude (Fig. 4c) and the values of σ^2 for the Eu-Sb and Eu-Os peaks are comparable ($\sigma \sim 0.06$ Å), which is expected for a rattler atom vibrating inside a nearly rigid cage. In contrast, the Nd-Os and Pr-Os peaks are significantly broadened ($\sigma \sim 0.13$ Å for Nd-Os and 0.12 Å for Pr-Os) and there is little amplitude where these peaks are expected. Because the second neighbor peak is expected to be much smaller than the first peak we compare the second neighbor region from 3.2-4.2 Å for the Nd and Eu samples in Fig. 5. To emphasize the small amplitude for Nd (and similarly for Pr), we have also calculated the second peak for the Nd sample (See purple, dot-dash line in top panel of Fig. 5) assuming the second peak has the same σ as the first peak as observed for $EuOs_4Sb_{12}$. Clearly there is significant excess disorder for the Nd-Os peak. In fact both the Nd and Pr LIII-edge data can be fit quite well over the 2.5-4.3 Å fit-range using only the first neighbor Nd-Sb or Pr-Sb FEFF functions.

Since the ultrasonic data[15–17] have been interpreted in terms of a significant 100 off-center displacement of Nd or Pr (Nd - 0.4 Å,[25] Pr - 0.2 Å[15]), we first simulated the low temperature data using these off-center results. In these simulations, both the Pr-Sb and Nd-Sb peak amplitudes were strongly reduced and the shape of all peaks changed. Thus a large 100 displacement is completely inconsistent with the EXAFS data. To check off-center models in more detail, we carried out fits assuming that the Nd or Pr atoms were displaced off-center along either the 100, 110, or 111 directions, within a rigid Os_4Sb_{12} cage. Here we follow the procedures we developed for off-center atoms in clathrates - see Ref. 36. Briefly, within a rigid cage assumption, all the Nd-Sb and Nd-Os distances can be expressed in terms of the off-center displacement, D, and the off-center direction.

For the 100 off-center model (six wells) there are five different Nd-Sb distances with amplitudes in the ratio 2:2:4:2:2. The distances can be written as $r_i = r_o + \alpha_i D$ where r_o is the Nd-Sb distance for Nd on-center and the slopes α_i are calculated for the different pairs with Nd off-center using FEFF8. There are four bonds shorter than r_o, four longer, while the Nd-Sb distance for the middle peak is almost unchanged. For this model the eight Nd-Os pairs separate into two groups of four, with pair distances that are shorter and longer than the nominal Nd-Os distance. Another set of slopes β_i define the Nd-Os distances in terms of D. Therefore allowing an off-center displacement introduces only one additional distance parameter. In addition, the broadening of the longer bonds is expected to be more than the shorter bonds and therefore several additional σ's were allowed to vary.

Similar models were considered for the other off-center displacement models. For 110, the most complicated model (twelve wells), the eight Ln-Sb amplitudes are in the ratio 1:2:1:2:2:1:2:1 but again all distances can be expressed in terms of D and eight slopes α_i, which were calculated using FEFF8. Here the eight Nd-Os pairs form three groups with amplitudes in the ratio of 2:4:2. Fi-

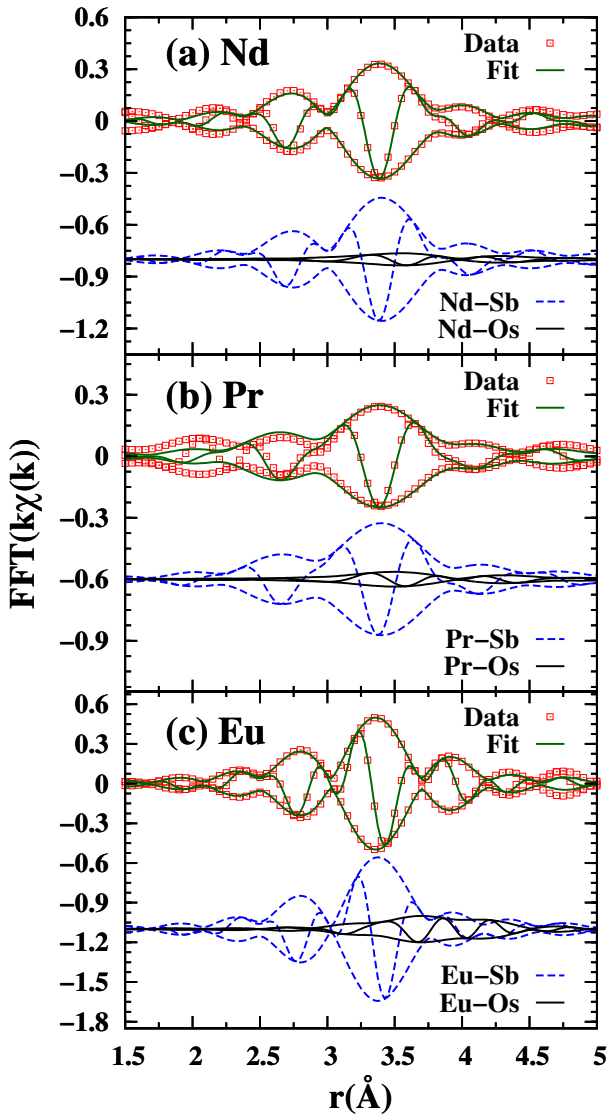

FIG. 4. Fits of the 4K data for each sample to a sum of two peaks, Ln-Sb and Ln-Os (Ln = Nd, Pr, Eu). The individual peaks obtained in the fits are also plotted and show that the first Ln-Sb peak dominates. The second neighbor peak (Nd-OS and Pr-Os) for Nd and Pr is surprisingly small.

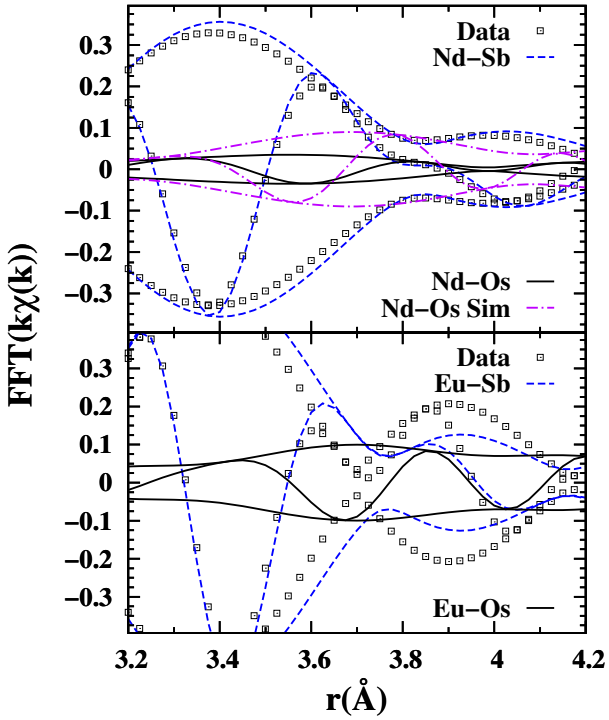

FIG. 5. (Color on-line) An expanded view of the second neighbor region comparing the Nd L_{III} data with that for Eu L_{III}. The data are shown as squares, the fit of the first peak as dashed (blue) lines and the fit for the second peak as a solid black line. Note that for Nd, the Nd-Sb first neighbor function extends above 4.2 Å, and already is close to the data over the r-range for the the second peak; the Nd-Os amplitude is low. In contrast for Eu, the Eu-Sb function is not close to the data above 3.5 Å, and the the Eu-Os function has a significant amplitude above 3.5 Å.

nally, for the 111 model (eight wells), the Nd-Sb distances are in four groups with amplitudes in the ratio 3:3:3:3 while the Nd-Os amplitudes are in the ratio 1:3:3:1. Identical models were used for the Pr off-center models.

Additional fits were carried out for each of the above models for the 4 K data. Surprisingly, there was very little improvement in the fits over the fit for an on-center model and in all cases D was small. Using Hamilton's F-test criteria,[37] the slight improvement using an off-center model is not significant for any model, and therefore, there is no statistical difference between an off-center model with a small off-center displacement and an on-center fit with a larger static disorder. More importantly, the off-center fits also resulted in some of the σ's for Nd-Sb or Pr-Sb pairs being smaller than expected for zero-point-motion (ZPM). It is well known that a static splitting of a peak leads to a broadening, $\sigma_{\rm static}$, of the pair distribution function,[35] but the thermal contributions to the broadening of each peak must still be above the ZPM value. Thus small σ's within an off-center model indicate that the off-center displacement used is too large. These fits place an upper limit to any off-center displacement, D $<$ 0.06 Å, which is less than the thermal vibration amplitude even at 75-100 K.

The important remaining anomaly is the low amplitude for the Nd-Os and Pr-Os peaks. Even within the off-center models, the fits make the σ's for Nd-Os and Pr-Os surprisingly large at 4 K. Thus, for the Nd and Pr samples there must be some other explanation for the extreme broadening. We return to this problem later.

To investigate the thermal vibrations of the rare earth rattler atoms, we fit the Ln L_{III}-edge data (Fig. 3), for temperatures from 4 to 300 K. From these fits we extracted σ(T), and in Fig. 6 we plot σ^2 as a function of T for each sample. σ^2 is well defined for the Ln-Sb neighbors and increases monotonically with T. The results are

TABLE II. Einstein temperatures, Θ_E, and static off-sets, σ^2_{static} for the first two peaks at the L_{III}-edge for Nd, Pr, and Eu. Estimated errors including systematics for Θ_E (K) are ±5 K; errors for $\sigma^2_{static} \sim 0.0004$ Å^2.

Atom pair	r (Å)	σ^2_{static}(Å^2)	Θ_E (K)
$NdOs_4Sb_{12}$			
Nd-Sb	3.483	0.00337	61
Nd-Os	4.030	0.0137	42
$PrOs_4Sb_{12}$			
Pr-Sb	3.480	0.00471	65
Pr-Os	4.027	0.00968	51
$EuOs_4Sb_{12}$			
Eu-Sb	3.487	0.00120	76
Eu-Os	4.035	0.00071	64

quite well described by an Einstein model as shown by the solid lines, leading to low Einstein temperatures Θ_E = 61, 65, and 76 K for the Nd-Sb, Pr-Sb and Eu-Sb peaks respectively. In this model, we have assumed that the Sb-Os cage structure is stiff (as found in the next sections) and only the rare earth atom is vibrating; hence the rattler motion is modeled as the rattler mass attached inside a rigid (infinite mass) cage. In this case, it is not correct to use the usual small reduced mass for say a Nd-Sb pair as the Sb atom is held fixed by the rest of the lattice. The actual reduced mass should be slightly less than the full rattler mass as discussed in Ref. 11 for the Eu rattler, but this effect is very small.

The low values of Θ_E for the first peak indicate that all the rare earth atoms are weakly bound within stiff skutterudite cages; Θ_E for the Eu-Sb peak is consistent with our previous EXAFS results.[11] The new value of Θ_E for Pr is a bit lower. More importantly the static off-sets at low temperature for Nd-Sb and Pr-Sb are fairly small and inconsistent with the large proposed off-center displacement of 0.4 Å for Nd,[25] in agreement with our unsuccessful attempts to fit to various off-center models discussed above. Generally there is some small static contribution to σ^2 from local strains; the small static off-sets from the fits are consistent with such local strain distortions.

The values of σ^2 for the second peaks are not as well defined because of the low peak amplitudes and therefore also have much larger errors, particularly for Nd-Os and Pr-Os. In addition, at high temperature these peaks, including the Eu-Os peak, become too low in amplitude to extract σ. For the Eu-Os peak, the values of σ^2(T) are very similar to those for the Eu-Sb peak but increase slightly faster with T; the calculated Einstein temperature is thus a bit smaller. These results are given in Table II. None of the previous EXAFS studies investigated σ^2(T) for the second neighbors.

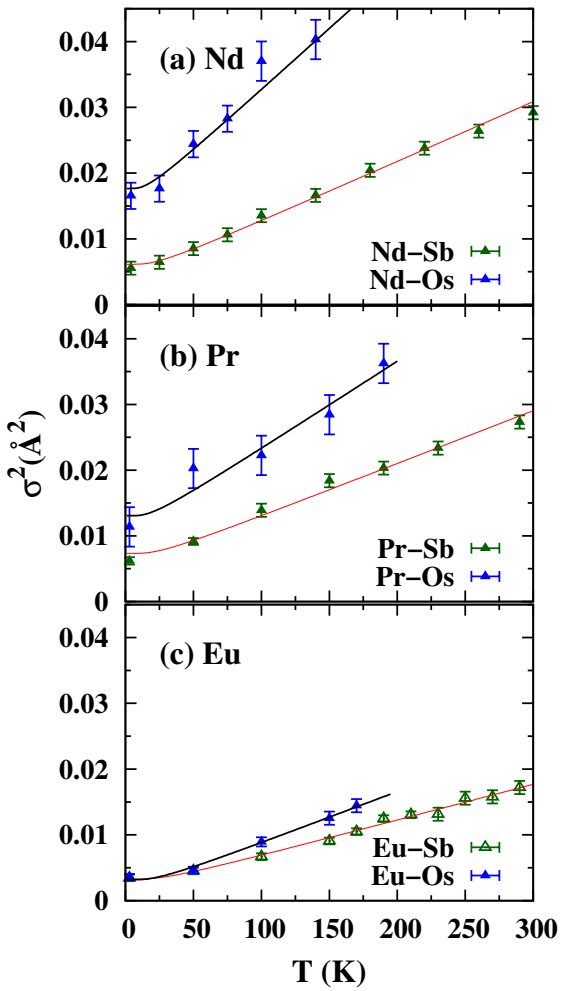

FIG. 6. σ^2(T) for the Ln-Sb and Ln-Os peaks, at the Ln L_{III}-edges for the $LnOs_4Sb_{12}$ samples (Ln = Nd, Pr, and Eu). Note that for Nd and Pr the values of σ^2 for the Ln-Os peak are large even at low T, while for the Eu sample, σ^2 is comparable for Eu-Sb and Eu-Os. The solid lines are fits to an Einstein model - see text and Table II.

B. Sb K-edge data

Next we considered the local distortions from the perspective of the Sb atoms. The Sb K-edge r-space data for the three samples are plotted in Fig. 7 (FT range 3.5-14 Å^{-1}) and show very similar spectra for each sample. The first few peaks are Sb-Os, and several Sb-Sb peaks - see Fig. 1; the weak Sb-Ln peak (one neighbor) is not visible because it is under the larger Sb-Sb peaks. The amplitudes of the Sb-Os and Sb-Sb peaks are high at low temperature and decreases slowly with temperature, indicative of moderately high, correlated Debye temperatures, and quite stiff effective spring constants. In particular, there is no obvious evidence for disorder in the Sb-Os bond.

We fit the data from 1.8-3.8 Å to a sum of five single

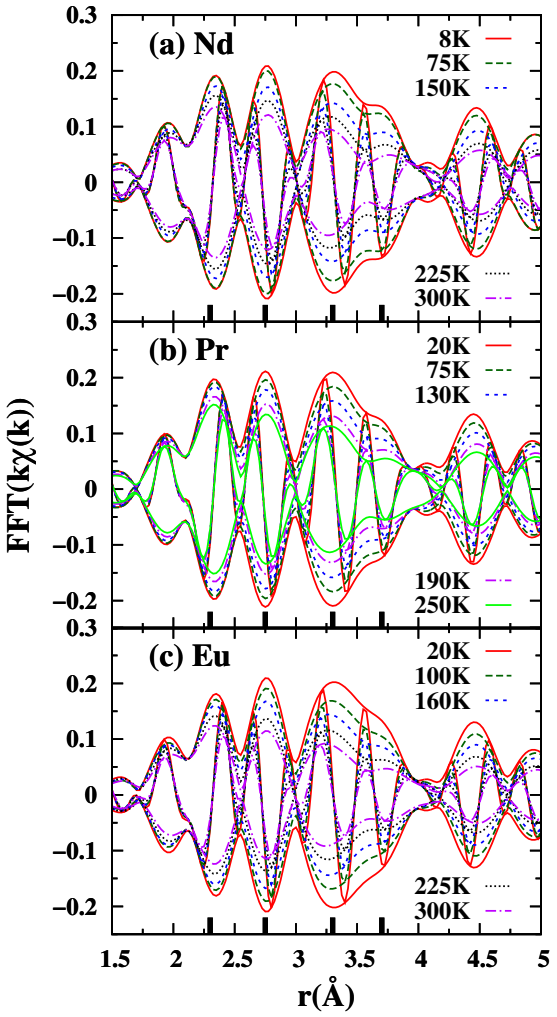

FIG. 7. Plots of the Sb K-edge r-space data vs temperature for $NdOs_4Sb_{12}$, $PrOs_4Sb_{12}$, and $EuOs_4Sb_{12}$; FT range 3.5-14 $Å^{-1}$. The plots are very similar and have large amplitudes indicating little distortion. The first peak is Sb-Os, the next three are Sb-Sb; the small Sb-Ln peaks are not visible as a separate peak and occurs near 3.3 Å; the EXAFS peak positions for Sb-O and three Sb-Sb peaks are indicated by short vertical lines for each sample.

scattering standards (calculated using FEFF8[34]); within this r-space fit-range there are no significant multi-scattering peaks. The ratios of the amplitudes were constrained to the crystal structure (i.e. the amplitude ratios were 2:2:1:4:4 — for the Os, first Sb, nearest Nd neighbor, second Sb, an abrupt Sb neighbors); note that the first Sb-Sb peak is actually the sum of two closely spaced peaks that cannot be resolved and we treat this first Sb-Sb peak as a single peak with two Sb neighbors. In these fits, only the first peak amplitude was allowed to vary to obtain S_o^2; $S_o^2 = 1.0$. For higher temperatures, all amplitudes were fixed using this value of S_o^2. Similarly the atom-pair distances were constrained to the structure with only an overall lattice constant allowed to

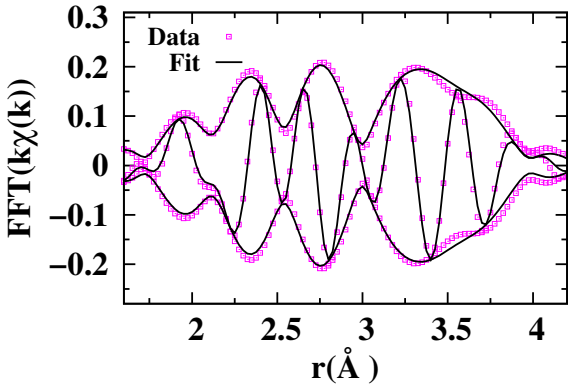

FIG. 8. An example of a fit of the Sb K-edge data at 8 K for the $NdOs_4Sb_{12}$ sample. Data are shown as filled squares with the fit given by the solid line. Five peaks were used for the fit. The r-space fit range is 1.8-3.8 Å. Same FT range as for Fig. 7.

vary. From preliminary fits, we found that σ for the small Sb-Nd peak and the overlapping Sb-Sb peak at 3.53 Å were highly correlated, and therefore constrained σ(T) for the Sb-Nd peak to be the same as for Nd-Sb from the Nd L_{III}-edge fit. This leads to consistent values of σ for the Sb-Sb peak at 3.53 Å. E_o was determined from the low temperature fits for each sample and then fixed for all higher T fits. In these fits, we only varied five parameters (four σs and one overall distance), much less than the number of independent parameters, 16.6, calculated using Stern's criteria,[38]. An example of such fits is shown in Fig. 8 for the Nd sample at 4 K. The resulting Sb-Os and Sb-Sb distances were approximately 0.01 Å shorter than the x-ray structure data, but this is within systematic uncertainties and indicates that there is no major distortion of the environment about the Sb atoms.

From these fits, we extracted σ(T) for the Sb-Os and the three Sb-Sb peaks; σ^2(T) for each pair is plotted in Fig. 9. All plots show a fairly weak temperature dependence, with the strongest T-dependence observed for the longest pairs ($\sim$ 3.88 Å) as expected. The σ^2(T) data for each peak were fit to a correlated Debye model - these results are show as solid lines on Fig. 9, and the correlated Debye temperatures, Θ_{cD}, and the static disorder, σ^2_{static}, are tabulated in Table III. The temperature dependencies of σ^2(T) and the values of σ^2_{static} for the various atoms pairs are similar for the three $LnOs_4Sb_{12}$ samples. Thus from the perspective of the Sb atoms, the structure agrees well with the average structure from diffraction.

C. Os L_{III}-edge data

Finally, we show the Os L_{III}-edge data for the same three samples in Fig. 10; the FT range is 4-14 $Å^{-1}$ for each sample. Here the first peak near 2.5 Å is due to the six nearest Sb neighbors, while the next large peak

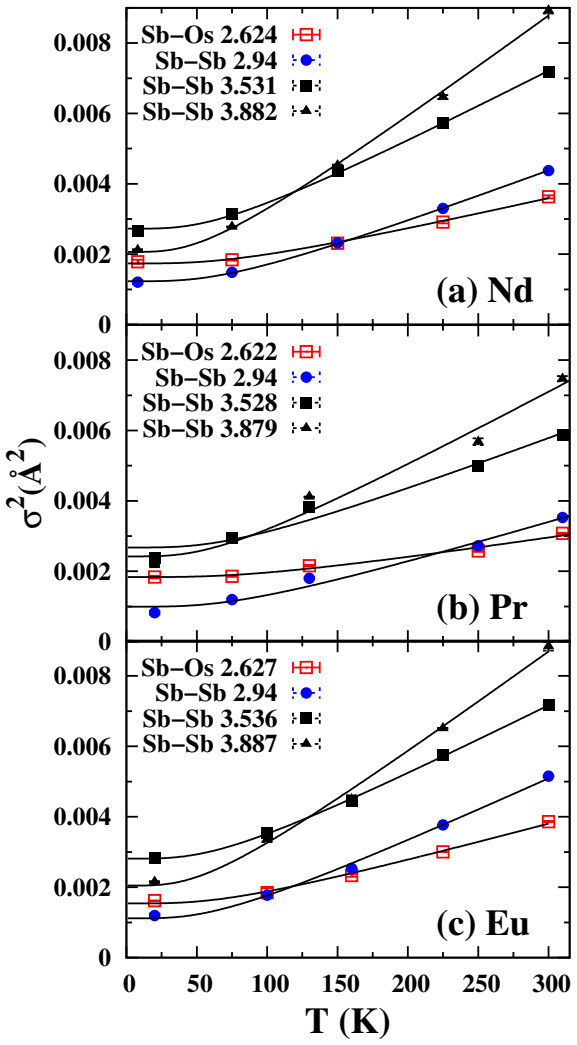

FIG. 9. σ^2(T) for the first few atom-pairs about Sb for $NdOs_4Sb_{12}$, $PrOs_4Sb_{12}$, and $EuOs_4Sb_{12}$. Correlated Debye fits for each peak are shown as solid lines.

near 4.2-4.5 Å is a sum of an Os-Sb and an Os-Os peak - see Fig. 1. The weak Os-Ln peak occurs near 3.6-3.7 Å, but is under the tail of the second Os-Sb peak. The temperature dependence is quite weak for the first Os-Sb pair and the peak still has a large amplitude at 300 K, indicating a stiff Os-Sb bond. For the more distant neighbors, the temperature dependence is considerably stronger, as expected.

The Os L_{III}-edge data were fit following the same procedures as described above with $S_o^2 = 0.92$; however the r-space fit range was longer, 2-4.7 Å, and only four peaks (Os-Sb, Os-Nd, second Os-Sb and Os-Os) were included, with the amplitude ratios constrained to 6:2:12:6. No significant multiscattering peaks occur within this fit range. Again the distances were constrained to the structure and only an overall lattice constant was allowed to vary. Thus only five parameters were varied - four σ's and one distance, while the number of independent parameters from

TABLE III. Pair distances, static disorder, $\sigma^2_{\rm static}$, and correlated Debye temperatures, $\Theta_{\rm cD}$, for the Sb-Os and three Sb-Sb peaks in each sample. The small static disorder is consistent with zero static disorder. Uncertainties in $\sigma^2_{\rm static}$ are often dominated by correlations between σ's for partially overlapping peaks and are typically ± 0.0004 Å^2. Because most correlated Debye temperatures are comparable to or above the highest temperature used to collect data (300 K), $\Theta_{\rm cD}$ is very sensitive to the highest temperature data point and the estimated systematic error is ± 30 K.

Atom pair	r(s) (Å)	$\sigma^2_{\rm static}$(Å^2)	$\Theta_{\rm cD}$(K)
NdOs4Sb12			
Sb-Os	2.624	0.00067	325
Sb-Sb	2.94	-0.00036	296
Sb-Sb	3.531	0.00074	277
Sb-Sb	3.88	-0.00034	240
PrOs4Sb12			
Sb-Os	2.622	0.00097	399
Sb-Sb	2.94	-0.00043	331
Sb-Sb	3.528	0.00097	323
Sb-Sb	3.879	0.00037	281
EuOs4Sb12			
Sb-Os	2.627	0.00038	299
Sb-Sb	2.94	-0.00064	268
Sb-Sb	3.536	0.00085	280
Sb-Sb	3.887	-0.00035	241

Stern's criteria[38] is ∼ 15. An example fit is shown in Fig. 11.

Fig. 12 shows σ^2(T) for two Os-Sb and the Os-Os atom pairs. All plots show a weak temperature dependence as expected for a rigid cage structure. The σ^2(T) data for each peak were fit to a correlated Debye model - except for the Os-Os peak in the $NdOs_4Sb_{12}$ and $PrOs_4Sb_{12}$ samples (see below); these results are shown as solid lines on Fig. 12, and the correlated Debye temperatures $\Theta_{\rm cD}$, and the static off-set $\sigma^2_{\rm static}$ are tabulated in Table IV. For $EuOs_4Sb_{12}$, the results show very little static disorder - consistent with little or no strain in the sample and no off-center effects. For $NdOs_4Sb_{12}$ and $PrOs_4Sb_{12}$, the results are similar for the two Os-Sb peaks, although there is a bit more static disorder for the Os-Sb pair at ∼ 4.54 Å.

However the σ^2(T) data for the Os-Os peak are not fit well by the correlated Debye model and there is significant excess static disorder at low temperature. Since the $NdOs_4Sb_{12}$ data have the best signal-to-noise and many more temperature points, we focus the discussion of the Os-Os peak on this sample. First, we consider the correlated Debye model fit to all the $\sigma^2_{\rm Os-Os}$(T) data for $NdOs_4Sb_{12}$ (solid line); note that all data points from 100-250 K are below the fit, while the 300 K point is well above it. Also note that below 50 K, $\sigma^2_{\rm Os-Os}$(T) appears to increase slightly, similar to the unusual behavior observed previously for $PrRu_4P_{12}$,[13] and the static off-set for the full fit is very large, ∼ 0.003 Å^2. If instead, we only fit the top four points (dotted line for Os-Os in Fig. 12a), then the correlated Debye temperature is somewhat lower (222 K) and the ZPM contribution to $\sigma^2(0)$ is also

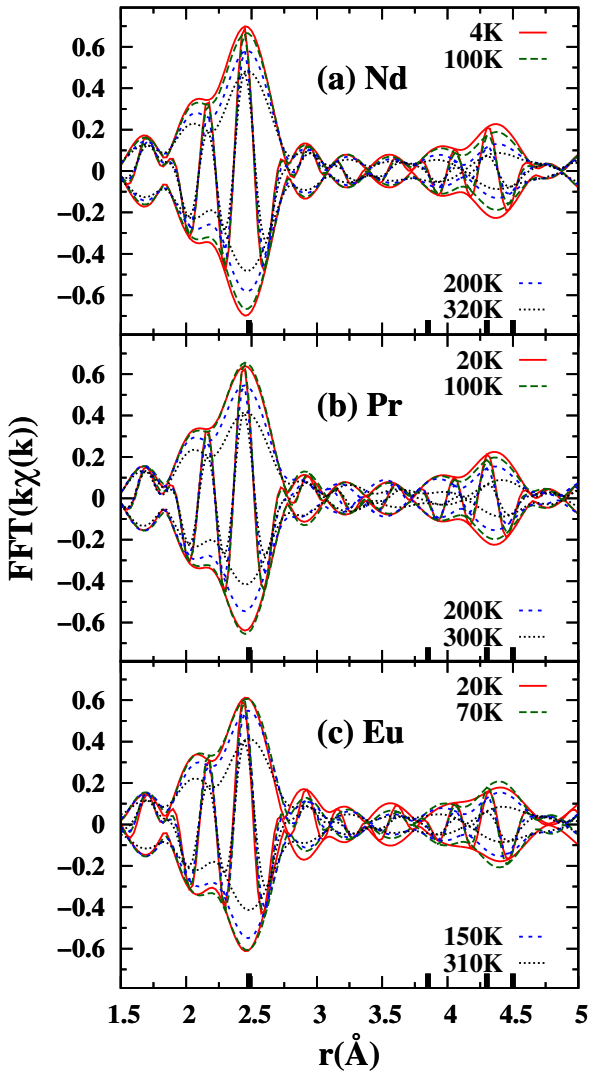

FIG. 10. The r-space data at the Os L_{III}-edge for $NdOs_4Sb_{12}$, $PrOs_4Sb_{12}$, and $EuOs_4Sb_{12}$; FT range, 4-14 $Å^{-1}$. The first large peak is Os-Sb near 2.5 Å; the Os-Sb (near 4.3 Å) and Os-Os ($\sim$ 4.5 Å) peaks partially overlap and form the large peak from 4.2-4.5 Å. The small Os-Ln peak is near 3.6-3.7 Å. The positions of these peaks on the EXAFS plots are shown as short vertical lines.

larger. Consequently σ^2_{static} would be lower (0.0157 $Å^2$). This suggests that the static disorder in the Os-Os PDF increases as T drops below $\sim$ 150 K and becomes constant near 40 K, close to the temperature at which the anomaly is observed in the ultrasonic measurements for $NdOs_4Sb_{12}$.[15]

For $PrOs_4Sb_{12}$, there are larger errors in σ^2(T) for the Os-Os pair and it appears that there is a step increase in σ^2 as T is decreased below 200 K. Although we do not consider this pair further, the temperature dependence of σ^2 for the Os-Os pair in $PrOs_4Sb_{12}$ has a similar behavior to that for the Nd sample.

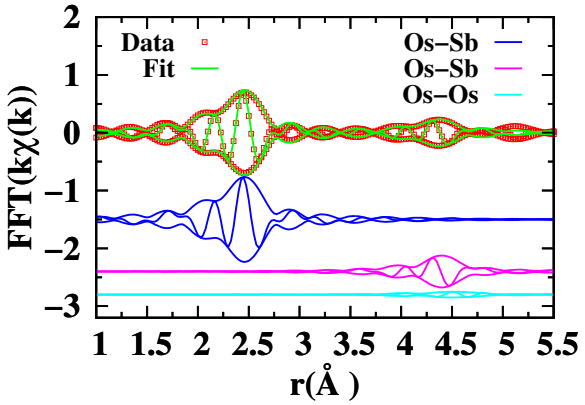

FIG. 11. The r-space data at 6 K and fits at the Os L_{III}-edge for $NdOs_4Sb_{12}$; FT range, 4-14 $Å^{-1}$. The data are presented as (red) squares with the total fit shown as a solid (green) line; we obtain an excellent fit up to 4.5 Å. Three shells of neighbors are shown below the fit (the Os-Nd is too weak to see on this scale). The second (blue) trace is the fit for the Os-Sb peak at 2.624 Å, the third (purple) trace is for the Os-Sb peak at 4.53 Å, and the tiny, fourth trace is the Os-Os peak at 4.654 Å.

TABLE IV. Pair distances, static disorder, σ^2_{static}, and correlated Debye temperatures, Θ_{cD}, for two Os-Sb and the Os-Os peaks in each sample. The small static disorder for the OS-Sb peaks is consistent with zero static disorder. Uncertainties in σ^2_{static} are $\sim \pm$ 0.0004 $Å^2$. Because most correlated Debye temperatures are comparable to 300 K, Θ_{cD} is very sensitive to the highest temperature data point and the estimated systematic error is $\pm$ 30 K except for the Os-Os peaks in a) and b).

Atom pair	r(s) (Å)	σ^2_{static} ($Å^2$)	Θ_{cD} (K)
$NdOs_4Sb_{12}$			
Os-Sb	2.624	0.0003	327
Os-Sb	4.53	0.00056	248
Os-Os	4.654	0.00277	257
$PrOs_4Sb_{12}$			
Os-Sb	2.622	0.00009	308
Os-Sb	4.53	0.00025	244
Os-Os	4.650	0.00252	255
$EuOs_4Sb_{12}$			
Os-Sb	2.627	0.00040	309
Os-Sb	4.54	0.00053	251
Os-Os	4.660	.00039	340

IV. DISCUSSION AND CONCLUSIONS

Our analysis of the Ln L_{III} EXAFS data show that, relative to the nearest Sb neighbors, the Nd, Pr, and Eu are all on-center and have similar vibrational behavior. The average pair distances also agree well with diffraction and the space group $Im\bar{3}$. All Ln-atoms are rattlers inside fairly rigid Os/Sb cages and have low Einstein temperatures; consequently all should scatter phonons well. The values of σ^2_{static} are quite small for Nd-Sb, Pr-Sb and very small for Eu-Sb. In addition, attempts to fit

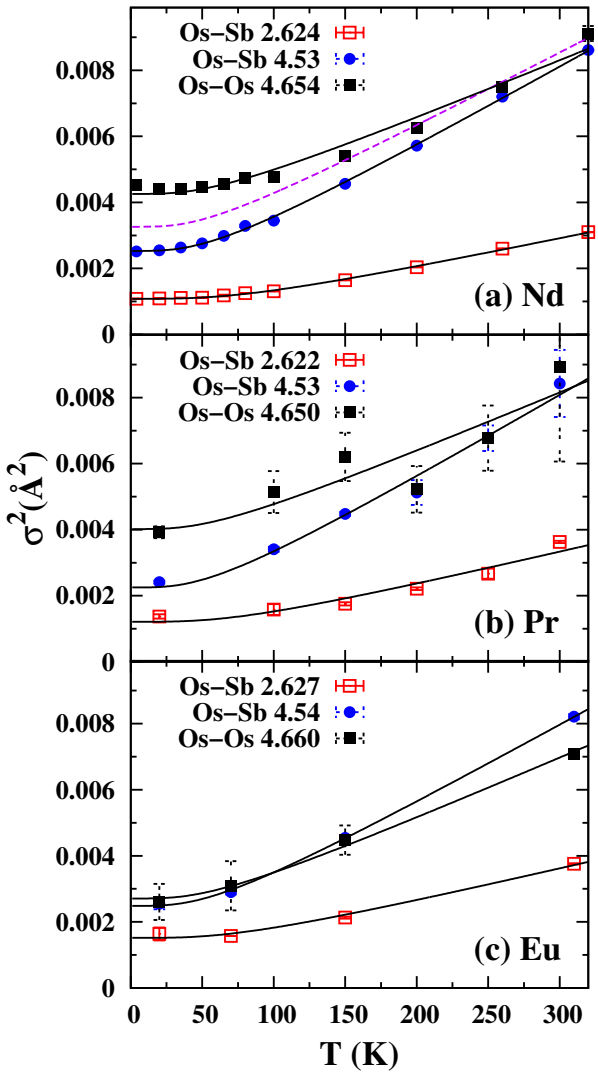

FIG. 12. σ^2(T) for Sb and Os neighbors about Os for $NdOs_4Sb_{12}$, $PrOs_4Sb_{12}$, and $EuOs_4Sb_{12}$; open squares (red) Os-Sb ($\sim$ 2.63 Å); filled circles (blue), Os-Sb ($\sim$ 4.54 Å); filled squares (black) Os-Os ($\sim$ 4.65 Å). Solid lines are correlated Debye model fits over the entire temperature range. Note the poor agreement between the data and the correlated Debye fit for the Os-Os pair in $NdOs_4Sb_{12}$ and $PrOs_4Sb_{12}$ compared to $EuOs_4Sb_{12}$. In a), a fit to only the four highest temperature points for $NdOs_4Sb_{12}$ is shown as a dotted line, and leads to a lower Θ_{cD} and a smaller value of σ^2_{static}.

the Nd-Sb and Pr-Sb data using off-center models with displacements along 111, 110 or 100, did not significantly improve the fits and lead to an off-center displacement of at most 0.06 Å. Thus we conclude that Nd and Pr are not significantly off-center, as proposed to explain ultrasonic data at low T.[15,16,25] On the basis of the EXAFS results, it would appear that another mechanism must be operative to explain the results of the ultrasonic measurements.

In contrast to the first neighbor peak, the second neighbor peaks corresponding to Ln-Os pairs are highly disordered at 4 K in $NdOs_4Sb_{12}$ and $PrOs_4Sb_{12}$i (i.e. σ^2_{static} is large), but not in $EuOs_4Sb_{12}$ - see Fig. 6. This indicates that other distortions of the lattice exist for the Nd and Pr samples, at least at low temperatures.

EXAFS data at the Sb K- and Os L_{III}-edges allows us to explore other possible distortions. From the perspective of the Sb atoms, the static disorder is quite small and consistent with random strains in the materials – see Fig. 9. There is a bit more static distortion for Sb-Os pairs in the Nd and Pr samples compared to the Eu sample, but the effect is small. The first few Sb-Sb peaks have quite small static disorder and moderately stiff bonds, consistent with a stiff Os/Sb cage around the Ln atoms.

For the Os L_{III}-edge data, the σ^2(T) plots show comparable disorder for the Os-Sb bonds in all three samples but a significantly larger distortion for the Os-Os pairs in the Nd and Pr samples compared to the Eu sample. The combined results indicate that the largest disorder is observed for the Nd-Os, Pr-Os, and Os-Os peaks in $NdOs_4Sb_{12}$ and $PrOs_4Sb_{12}$, with a smaller distortion for Sb-Os pairs. All the peaks in $EuOs_4Sb_{12}$ and the other peaks for the Nd and Pr samples show typical behavior.

Before considering possible models to explain the EXAFS data, it is first useful to contrast/compare with other structural measurements and attempt to include those results in forming a model. We first start with experiments that characterize the rattler vibrations in terms of an Einstein temperature and a static off-set. In EXAFS, σ^2_{Ln-Sb}(T) for the Ln-Sb pair is given by:

$$\sigma^2_{Ln-Sb}(T) = \sigma^2_{static} + \frac{\hbar^2}{2\mu k_B \Theta_E} \coth \frac{\Theta_E}{2T}, \qquad (2)$$

while in diffraction the isotropic thermal parameter U_{iso}(T) (here for the rare arth atom) is given by

$$U_{iso}(T) = u^2_o + \frac{\hbar^2}{2m k_B \Theta_E} \coth \frac{\Theta_E}{2T}, \qquad (3)$$

where μ is the effective mass of the Einstein oscillator in EXAFS, m is the mass of the rattler atom in diffraction experiments, Θ_E is the Einstein temperature, and σ^2_{static} and u^2_o are the static off-sets in EXAFS and diffraction, respectively. Although in many systems the effective mass for EXAFS is calculated from the two atoms involved, that is not appropriate here; the cage is quite rigid and effectively has a large cage mass. In the limit of a large rigid cage, then $\mu = m$, the rattler mass, and Eqns. 2 and 3 are essentially identical - i.e because the Sb atom is held firmly within the Os_4Sb_{12} lattice, the relative vibration of the Ln-Sb pair is primarily the vibration of the central Ln atom, and in this special case σ^2 from EXAFS should be similar to U_{iso} from diffraction. There is still one important difference – σ^2_{Ln-Sb}(T) is a measure of vibrations along the Ln-Sb direction, whereas U_{iso}(T) is an average over all directions. Since the vibrations

TABLE V. Comparison between Einstein temperatures (Θ_E) and the static off-sets - called σ^2_{static} (or C_2^2) in EXAFS and u_o^2 in diffraction. Note: for Ref. 24 there appears to be a typo in their Table II and we have used values of u_o from their Fig. 6 for Nd and Pr. Furthermore, they use a high temperature approximation for the Einstein model; extrapolation to T=0 often gives an intercept larger than u_o^2.

	EXAFS (Nitta)[14]		Diff. (Yamaura)[24]		This work	
Atom	Θ_E(K)	σ^2_{static}(Å^2)	Θ_E(K)	u_o^2 (Å^2)	Θ_E(K)	σ^2_{static} (Å^2)
Nd	134	0.107	47	0.013	61	0.0034
Pr	127	0.078	59	0.011	65	.0047

TABLE VI. Atomic coordinates for the space group $Pm\bar{3}$ where x is the variable that describes the degree to which the structure deviates from $Im\bar{3}$. If x = 0, and for the Sb sites, y = y' and z = z', one obtains the same positions as for the $Im\bar{3}$ space group. For $PrRu_4P_{12}$ which takes the $Pm\bar{3}$ space group at low temperatures,[40,41] x is very small, $\sim$ 0.0007.

Atom	Site	x	y	z
Nd(1)	1a	0	0	0
Nd(2)	1b	0	0.5	0.5
Os	8i	0.25+x	0.25+x	0.25+x
Sb(1)	12j	0	y	z
Sb(2)	12k	0.5	0.5+y'	-0.5+z'

may be larger in directions where there are no Sb neighbors - i.e. towards voids in the Sb cage, then the average mean square vibrations for U_{iso}(T) might be larger than σ^2_{Ln-Sb}(T) - and the corresponding Θ_E, slightly smaller.

As T goes to zero, $\sigma^2_{Ln-Sb}(0)$ or $U_{iso}(0)$ is the sum of two constant terms;

$$\sigma^2_{Ln-Sb}(0) = \sigma^2_{static} + \sigma^2_{ZPM}$$
$$U_{iso}(0) = u_o^2 + u^2_{ZPM} \quad (4)$$

where $\sigma^2_{ZPM} = u^2_{ZPM} = \hbar^2/(2mk_B\Theta_E)$. Here, ZPM refers to zero-point-motion; σ^2_{ZPM} is quite large for systems with a small Θ_E. Also note that the value of σ^2_{static} depends on the value of Θ_E used – if Θ_E is large, then σ^2_{ZPM} is small and more of the value of $\sigma^2(0)$ is associated with static distortion. Thus, it is crucial to use the correct value of Θ_E to estimate the static contributions. In Table V we summarize some results from various experiments for the Nd and Pr rattlers in $NdOs_4Sb_{12}$ and $PrOs_4Sb_{12}$.

First note that our values of values of Θ_E for Nd and Pr (61 and 65 K) agree quite well with the diffraction results (47 and 59 K), considering that the Θ_E values for diffraction should be somewhat smaller because U_{iso} refers to an isotropic average. The values of of u_o^2 from diffraction are somewhat larger than our results - but as noted in the Table caption, their use of the high temperature approximation for the Einstein model equation can overestimate the static contributions.

The main disagreement is with Nitta *et al.*'s EXAFS results, where they report Θ_E to be 134 and 127 K – see Table V. Much of this discrepancy is due to using the Ln-Sb reduced mass instead of the rattler mass. Sb is slightly lighter than the rare earth masses (123 for Sb vs 140 and 144 for Pr and Nd, respectively); consequently, the Ln-Sb reduced mass is about a factor of two smaller than the rattler masses. In addition, the much larger values of Θ_E also increases their estimate of the static distortions; if Θ_E is large, then σ^2_{ZPM} will be small and σ^2_{static} contribution must be correspondingly larger - see Equ. 4. In addition there is a significant difference in their k-space data compared to ours. In our k-space data the amplitudes for Nd and Pr L_{III} traces are very similar, while for Nitta *et al.*[14] the amplitude for the Nd sample is considerably smaller than for Pr, particularly above k = 7 Å^{-1}. Thus the very large values of σ^2_{static} they report are in part a consequence of the large value of Θ_E and an overall increased disorder in their $NdOs_4Sb_{12}$ sample. Unfortunately they do not provide enough details to make a more detailed comparison; although they appear to fit more than one neighbor, they do not report any results for Nd-Os or Pr-Os.

Other diffraction results,[24,39] particularly the neutron scattering measurements,[24] show that the nuclear density about the rattler site is not spherical but is slightly peaked towards the Os atoms (111 direction) at high temperatures. This is the same direction for which we see excess distortion for the Nd-Os and Pr-Os pairs - so it is likely related.

The above comparisons show considerable agreement between our EXAFS results and diffraction, and we have suggested a plausible explanation for the disagreement with another EXAFS experiment.[14] Thus we conclude that there is little evidence for off-center displacements of the rattler atoms or unusual distortions of the Ln-Sb PDF. Extending our analysis out to several shells of neighbors suggests that the Ln-Os PDF and also the Os-Os PDF have excess static distortion, while other pair distributions have little excess distortion.

What distortions might lead to these particular pairs being distorted? Studies of $PrRu_4P_{12}$[13,40,41] suggest one possibility: in that material, the Ru-Ru peak becomes split at low temperature leading to a metal/insulator transition near 60 K, and the structure can be modeled using the $Pm\bar{3}$ space group instead of the usual $Im\bar{3}$ space group for the skutterudites. The atomic positions for this space group are shown in Table VI. The most important difference is that the Os positions are at (0.25+x,0.25+x,0.25+x), with x determining the deviation from $Im\bar{3}$ (x = 0 corresponds to $Im\bar{3}$). Applying this scenario to the $LnOs_4Sb_{12}$ systems, the two main effects are a splitting of the Ln-Os distances and the Os-Os distances, with a much smaller splitting of the Sb-Os distances. In Fig. 13, we show the structure for an exaggerated example of the change, with a focus on the Os positions (i.e. x is large for the Os positions). The figure shows large and small Os cubes about each Ln atom - see also Fig. 4 in Ref. 41. To see how these splittings vary

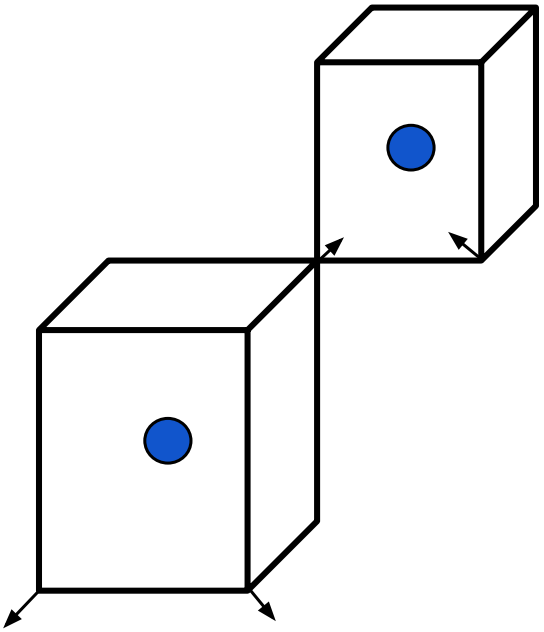

FIG. 13. The change in skutterudite structure for the $Pm\bar{3}$ space group showing two different sized cubes of Os atoms around the Ln atoms, along a 111 axis. The displacement x is large to show how one cube is enlarged and the other contracted.

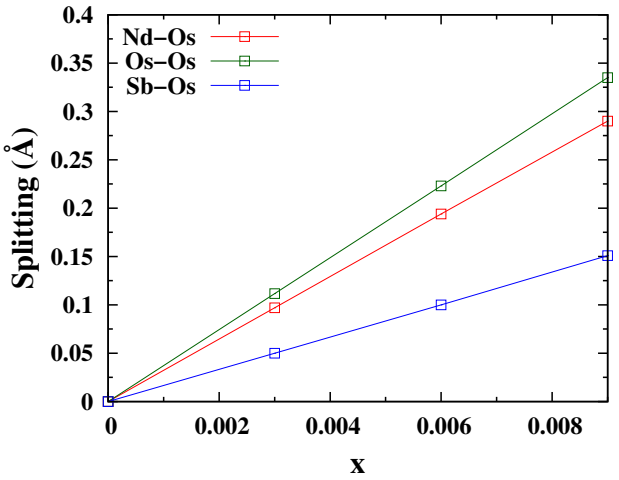

FIG. 14. Splitting for the Os-Os, Os-Sb, and Os-Nd peaks as a function of the displacement x in the $Pm\bar{3}$ space group. The splittings are comparable for Nd-Os and Os-Os pairs while that for the Sb-Os pair is roughly half as large. Note that to first order, Nd-Sb and Sb-Sb peaks are not affected by the increase in x under the approximation that y = y' and z = z'.

we plot them for the Os-Os, Ln-Os, and Os-Sb pairs in Fig. 14 as a function of x. For small x, the splittings are linear in x; the Os-Os and Ln-Os splittings are comparable while the Os-Sb splitting is about a factor of two smaller.

A second type of possible distortion that would lead

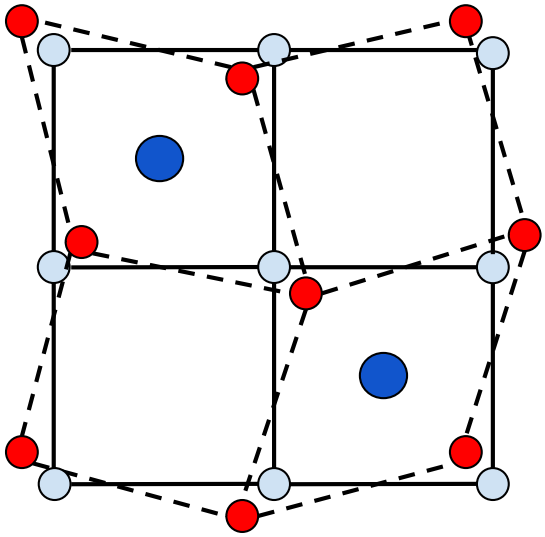

FIG. 15. A distortion of a skutterudite unit cell (viewed along a 001 axis) that keeps the Os-Os distance constant but splits the Ln-Os distances into four longer and four shorter distances. Large atoms - Ln; Sb atoms not shown for clarity.

primarily to long and short Ln-Os distances, but no change in the Os-Os distances, is illustrated in Fig. 15 looking down a 100 axis. It is a distortion in which the Os cubes surrounding an Ln atom in the skutterudite structure are slightly sheared so that two cube-faces are distorted from squares to parallelograms.

Note that the EXAFS results indicate a gradual structural change as T is lowered below $\sim$ 150 K - i.e. it appears that the static (or quasi-static) disorder observed at low temperature is not present at high T; otherwise, the fit of the Os-Os data would have been better in Fig. 12. Also the diffraction experiments show no unusual behavior for Os, although there was little focus on the Os atom positions. In contrast, the ultrasonic data show a sudden change in elastic constants at low temperature suggesting an abrupt change in structure. This may indicate a dynamic effect because EXAFS is very fast (10^{-16} s time scale) and observes all distortions, while ultrasonic measurements are on relatively slow time scales. If the structure is distorting dynamically, EXAFS will observe all the distortions but ultrasonics may not be sensitive to such distortions until the fluctuations are slower than the ultrasonic time scale. There may well be a mixture of the two distortions discussed above, particularly if the distortions are fluctuating rapidly, or a distribution of such distortions. In that case the EXAFS results indicate the following splittings from the magnitudes of $\sigma^2_{\rm static}$ for various atom pairs. The distortions for the Os-Os and Os-Sb are roughly consistent with the distortions present within a $Pm\bar{3}$ structure for x $\sim$ 0.003; a splitting of the Os-Os distances of roughly 0.1 Å (i.e. r = $r_o \pm$ 0.05 Å) and a possible small splitting of the Sb-Os peak of 0.03-0.05 Å. However, the experimental splitting for Nd-Os to explain the large value of $\sigma^2_{\rm static}$ for this pair is about a factor of

two larger, - $\sim$ 0.2 Å. Thus, if roughly half the disorder of the Nd-Os pair came from the $Pm\bar{3}$ structure and half arose from a further distortion as pictured in Fig. 15, then the excess EXAFS distortions could be explained. It is not clear how much such distortions would change the elastic constants. Another possibility is suggested by the diffraction results[24] which suggest that vibrations of the rattler are larger towards Os than towards Sb at least at high T. If that is also true at low T, then the ZPM vibrations will also be anisotropic, and larger along 111. Then, less displacement of Os is needed to explain the large $\sigma^2_{\rm static}$ for Nd-Os (and Pr-Os). Thus, it is not clear if a dynamic $Pm\bar{3}$ distortion is sufficient to explain the disorder of the further neighbors or an additional distortion, as suggested in Fig. 15 is required.

It is not clear why the Nd and Pr samples have this unusual distortion whereas Eu does not; unfortunately earlier EXAFS analyzes have not explored distortions beyond the first neighbor pair. However we are just completing a detailed study of CeT_4As_{12} (T = Fe, Ru, and Os) at all edges and find no significant distortions in this Ce-As family of compounds; the results are very similar to those for $EuOs_4Sb_{12}$, except the Einstein and correlated Debye temperatures are higher as expected for the smaller unit cell.[42] Thus in our opinion it is the Nd and Pr samples that are unusual. Earlier work on the $PrRu_4P_{12}$ system[13,40,41] indicated that the skutterudite structure can have the distortion shown in Fig. 13 for space group $Pm\bar{3}$, and the distortions for the $NdOs_4Sb_{12}$ and Pr Os_4Sb_{12} compounds may be additional examples. Eu does have a lower valence (Eu is +2; Nd and Pr are +3) but the bond lengths for Nd-Sb, Pr-Sb and Eu-Sb differ by less than 0.01 Å; consequently it is unlikely that valence plays an important role.

Disorder in the structure of the Os/Sb cage network, either static or dynamic, will scatter phonons and electrons, reducing both the thermal (κ) and electrical ($\sigma_{\rm e}$) conductivities. Although a reduced thermal conductivity is desirable to increase the thermoelectric figure of merit $ZT = TS^2\sigma_{\rm e}/\kappa$, a reduced electrical conductivity is not. Thus, materials that show such disorder are less suitable for thermoelectric applications. If the entire material has a static change to a different crystal space group then, although the local displacements are different, the crystal would have long range order and there should be no increase in scattering from a change in crystal structure. The fact that these materials have considerable structural disorder, but not off-center displacements of Nd or Pr, needs to be included in any modeling of physical properties.

ACKNOWLEDGMENTS

This work was supported under NSF grant DMR1005568. The experiments were performed at SSRL, operated by the DOE, Division of Chemical Sciences. Sample synthesis and characterization at UCSD were supported by the US Department of energy under Grant No. DEFG02-04ER46105

[1] V. Keppens, D. Mandrus, B. C. Sales, B. C. Chakoumakos, P. Dai, R. Coldea, M. B. Maple, D. A. Gajewski, E. J. Freeman, and S. Bennington, Nature **395**, 876 (1998).

[2] B. C. Sales, in Handbook on the Physics and Chemistry of Rare Earths, edited by L. Eyring, K. A. Gschneidner, and G. H. Lander (Elsevier Science Publishing Co., Montana, 2002), vol. 33, p. 211.

[3] R. E. Baumbach and M. B. Maple, in Encyclopedia of Materials: Science and Technology, edited by K. Buschow, R. Cahn, M. Flemmings, and B. Ilschner (Elsevier, Oxford, 2010), pp. 1–6.

[4] M. B. Maple, E. D. Bauer, N. A. Frederick, P.-C. Ho, W. M. Yuhasz, and V. S. Zapf, Physica B **328**, 29 (2003).

[5] M. B. Maple, Z. Henkie, W. M. Yuhasz, P.-C. Ho, T. Yanagisawa, T. A. Sayles, N. P. Butch, J. R. Jeffries, and A. Pietraszko, J. Magn. Matter **310**, 182 (2007).

[6] K. Hattori, Y. Hirayama, and K. Miyake, Journal of the Physical Society of Japan **74**, 3306 (2005).

[7] S. Yashiki, S. Kirino, K. Hattori, and K. Ueda, J. Phys. Soc. Jpn. 80 **80**, 130 (2011).

[8] Y. Aoki, H. Sugawara, H. Harima, and H. Sato, J. Phys. Soc. Jpn. **74**, 209 (2005).

[9] H. Sato, D. Kikuchi, K. Tanaka, M. Ueda, H. Aoki, T. Ikeno, S. Tatsuoka, K. Kuwahara, Y. Aoki, M. Koghi, et al., J. Phys. Soc. Japan **77**, 1 (2008).

[10] M. Maple, Z. Henkie, R. Baumbach, T. Sayles, N. Butch, P.-C. Ho, T. Yanagisawa, W. Yuhasz, R. Wawryk, T. Cichorek, et al., J. Phys. Soc. Japan **77**, 7 (2008).

[11] D. Cao, F. Bridges, P. Chesler, S. Bushart, E. D. Bauer, and M. B. Maple, Phys. Rev. B **70**, 094109 (2004).

[12] E. D. Bauer, A. Slebarski, N. Frederick, W. Yuhasz, M. Maple, D. Cao, F. bridges, G. Giester, and P. Rogl., J. Phys. Con. Matt. **16**, 5095 (2004).

[13] D. Cao, R. H. Heffner, F. Bridges, I.-K. Jeong, E. D. Bauer, W. M. Yuhasz, and M. B. Maple, Phys. Rev. Lett. **94**, 036403/1 (2005).

[14] K. Nitta, Y. Omori, D. Kikuchi, T. Miyanaga, K. Takegahara, H. Sugawara, and H. Sato, J. Phys. Soc. Jpn. **77**, 063601 (2008).

[15] T. Yanagisawa, W. M. Yuhasz, P.-C. Ho, M. B. Maple, H. Watanabe, Y. Yasumoto, Y. Nemoto, and T. Goto, Physica B **403**, 735 (2008).

[16] T. Yanagisawa, P.-C. Ho, W. M. Yuhasz, M. B. Maple, Y. Yasumoto, H. Watanabe, Y. Nemoto, and T. Goto, J. Phys. Soc. Jpn. **77**, 074607 (2008).

[17] T. Yanagisawa, Y. Ikeda, H. Saito, H. Hidaka, H. Amitsuka, K. Araki, M. Akatsu, Y. Nemoto, T. Goto, P.-C. Ho, et al., J. Phys. Soc. Jpn. **80**, 043601 (2011).

[18] K. Matsuhira, C. Sekine, M. Wakeshima, Y. Hunatsu, T. Namiki, K. Takeda, I. Shirotani, H. Sugawara, D. Kikuchi, and H. Sato, J. Phys. Soc. Jpn. **78**, 124601 (2009).

[19] N. Ogita, T. Kondo, T. Hasegawa, Y. Takasu, M. Udagawa, N. Takeda, K. Ishikawa, H. Sugawara, D. Kikuchi, H. Sato, et al., Physica B **383**, 128 (2006).

[20] S. Tsutsui, H. Uchiyama, J. P. Sutter, A. Q. R. Baron, H. Sugawara, J. Yamamaura, Z. Hiroi, and A. Ochiai, Journal of Physics Conference Series **200**, 012213 (2010).

[21] C. H. Lee, I. Hase, H. Sugawara, H. Yoshizawa, and H. Sato, J. Phys. Soc. Jpn. **75**, 123602 (2006).

[22] R. P. Hermann, R. Jin, W. Schweika, F. Grandjean, D. Mandrus, B. C. Sales, and G. J. Long, Phys. Rev. Lett. **90**, 135505 (2003).

[23] G. J. Long, R. P. Hermann, F. Grandjean, E. E. Alp, W. Sturhahn, C. E. Johnson, D. E. Brown, O. Leupold, and R. Ruffer, Phys. Rev. B **71**, 140302 (2005).

[24] J. Yamaura and Z. Hiroi, J. Phys. Soc. Jpn. **80**, 054601 (2011).

[25] T. Goto, Y. Nemoto, K. Sakai, T. Yamaguchi, M. Akatsu, T. Yanagisawa, H. Hazama, K. Onuki, H. Sugawara, and H. Sato, Phys. Rev. B **69**, 180511(R) (2004).

[26] E. D. Bauer, N. A. Frederick, P.-C. Ho, V. S. Zapf, and M. B. Maple, Phys. Rev. B **65**, 100506(R) (2002).

[27] P.-C. Ho, W. M. Yuhasz, N. P. Butch, N. A. Frederick, T. A. Sayles, J. R. Jeffries, M. B. Maple, J. B. Betts, A. H. Lacerda, P. Rogl, et al., Phys. Rev. B **72**, 094410 (2005).

[28] E. A. Goremychkin, R. Osborn, E. D. Bauer, M. B. Maple, N. A. Frederick, W. M. Yuhasz, F. M. Woodward, and J. W. Lynn, Phys Rev. Let. **93**, 157003 (2004).

[29] H. Tou, Y. Inaoka, M. Doi, M. Sera, K. Asaki, H. Kotegawa, H. Sugawara, and H. Sato, J. Phys. Soc. Jpn. **80**, 074703 (2011).

[30] N. A. Frederick, T. D. Do, P. C. Ho, N. P. Butch, V. S. Zapf, and M. B. Maple, Phys. Rev. B **69**, 024523 (2004).

[31] Y. Jiang, F. Bridges, M. A. Avila, T. Takabatake, J. Guzman, and G. Kurczveil, Phys. Rev. B **78**, 014111 (2008).

[32] C. H. Booth, R-Space X-ray Absorption Package (????), http://lise.lbl.gov/RSXAP/.

[33] J. A. Victoreen, J. Appl. Phys. **20**, 1141 (1949).

[34] A. L. Ankudinov, B. Ravel, J. J. Rehr, and S. D. Conradson, Phys. Rev. B **58**, 7565 (1998).

[35] B. K. Teo (Springer-Verlag, New York, 1986).

[36] R. Baumbach, F. Bridges, L. Downward, D. Cao, P. Chesler, and B. Sales, Phys. Rev. B **71**, 024202 (2005).

[37] L. Downward, C. H. Booth, W. W. Lukens, and F. Bridges, AIP Conference Proceedings **882**, 129 (2007).

[38] E. A. Stern, Phys. Rev. B **48**, 9825 (1993).

[39] K. Kaneko, N. Metoki, H. Kimura, Y. Noda, T. Matsuda, and M. Kohgi, Journal of the Physcial Soc. of Jpn. **78**, 074710 (2009).

[40] C. H. Lee, H. Matsuhata, A. Yamamoto, T. Ohta, H. Takazawa, K. Ueno, C. Sekine, I. Shirotani, and T. Hirayama, J. Phys.-Condens. Mat. **13**, L45 (2001).

[41] C. H. Lee, H. Matsuhata, H. Yamaguchi, C. Sekine, K. Kihou, and I. Shirotani, J. Magn. Magn. Mater. **272-276**, 426 (2004).

[42] B. Car, F. Bridges, R. Baumbach, and M. B. Maple, unpublished.